HHS Public Access

Author manuscript

J Neurochem. Author manuscript; available in PMC 2017 November 01.

Published in final edited form as:

J Neurochem. 2016 November ; 139(4): 659–675. doi:10.1111/jnc.13840.

Imaging Mass Spectrometry Reveals Loss of Polyunsaturated Cardiolipins in the Cortical Contusion, Hippocampus and Thalamus after Traumatic Brain Injury

L. J. Sparvero[1,2,*], **A. A. Amoscato**[1,2,*], **A. B. Fink**[1,2], **T. Anthonymuthu**[3], **L.E. New**[3], **P.M. Kochanek**[3], **S. Watkins**[4], **V.E. Kagan**[1,2,#], and **H. Bayır**[1,2,3,#]

[1]Department of Environmental and Occupational Health, University of Pittsburgh, Pittsburgh, Pennsylvania

[2]Center for Free Radical and Antioxidant Health, University of Pittsburgh, Pittsburgh, Pennsylvania

[3]Department of Critical Care Medicine, and Safar Center for Resuscitation Research, University of Pittsburgh, Pittsburgh, Pennsylvania

[4]Department of Cell Biology, University of Pittsburgh, Pittsburgh, Pennsylvania

Abstract

Traumatic brain injury (TBI) leads to changes in ion fluxes, alterations in mitochondrial function and increased generation of reactive oxygen species, resulting in secondary tissue damage. Mitochondria play important signaling roles in coordination of multiple metabolic platforms in addition to their well-known role in bioenergetics. Mitochondrial signaling strongly depends on cardiolipin (CL), a mitochondria-specific structurally unusual anionic phospholipid containing four fatty acyl chains. While our previous reports indicated that CL is selectively oxidized and presents itself as a target for the redox therapy following TBI, the topography of changes of CL in the injured brain remained to be defined. Here we present a MALDI imaging study which reports regio-specific changes in CL, in a controlled cortical impact (CCI) model of TBI in rats. MALDI imaging revealed that TBI caused early decreases in CL in the contusional cortex, ipsilateral hippocampus and thalamus with the most highly unsaturated CL species being most susceptible to loss. Phosphatidylinositol was the only other lipid species that exhibited a significant decrease, albeit to a lesser extent than CL. Signals for other lipids remained unchanged. This is the first study evaluating the spatial distribution of CL loss after acute brain injury. We propose that the CL loss may constitute an upstream mechanism for CL-driven signaling in different brain regions as an early response mechanism and may also underlie the bioenergetic changes that occur in hippocampal, cortical and thalamic mitochondria after TBI.

Graphical Abstract

[#]Corresponding authors for proofs and reprints: Hülya Bayır, MD; bayihx@ccm.upmc.edu, Address: Children's Hospital of Pittsburgh., 4401 Penn Avenue, Pittsburgh, PA 15224. Valerian E. Kagan, PhD; kagan@pitt.edu, Address: Bridgeside Point, 100 Technology Drive, Room 330, Pittsburgh, PA 15219-3130.

[*]These authors contributed equally to the work.

Competing financial interests: The authors declare no competing financial interests.

Traumatic brain injury (TBI) leads to changes in ion fluxes and alterations in mitochondrial function.

Mitochondrial signaling strongly depends on cardiolipin (CL), which is selectively oxidized and presents itself as a target for redox therapy following TBI.

We describe a mass spectrometric lipid imaging study that reports regio-specific changes in rat brain CL in a controlled cortical impact (CCI) model of traumatic brain injury (TBI). While MALDI-MS imaging revealed that TBI caused decreases in CL in the contusional area 3 h after injury, it also revealed decreases extending well beyond the area of impact into histologically normal tissue in the hippocampus and thalamic regions. The more unsaturated CL species were most susceptible to loss.

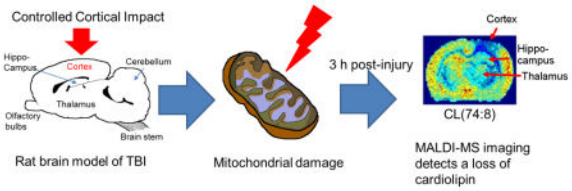

Introduction

Acute brain injury from trauma affects more than 1.5 million people every year in the United States alone (Faul *et al.* 2010; Mussack *et al.* 2002; Centers for Disease Control 2013). Progress in management of critically ill neurological patients has led to improved survival rates after traumatic brain injury (TBI); however, only ~ 40% of patients sustaining severe TBI will attain either moderate or good recovery in their long-term follow-up (Faul *et al.* 2010; Mussack *et al.* 2002; Centers for Disease Control 2013). The lifelong cost for continued care of a moderately to severely disabled person can exceed millions of dollars (Faul *et al.* 2010; Mussack *et al.* 2002; Centers for Disease Control 2013). Therapies that prevent morbidity, improve neurological outcome and quality of life in victims of TBI are desperately needed. Studies in experimental TBI revealed that the cortex, hippocampus and thalamus are selectively vulnerable to injury (Colicos, *et al.* 1996; Geddes *et al.* 2003; Sato *et al.* 2001; Tang *et al.* 1997). Previous studies reported alterations in the lipid profile as an important contributor to this vulnerability and the evolution of secondary damage in TBI (Bazan 2006; Hall, *et al.* 2010; Lewen *et al.* 2000). Subsequent to this, other studies have provided essential information on the spatial distribution of the altered lipid profile in response to traumatic brain injury, blast injury and ischemia/reperfusion injury (Roux *et al.* 2016; Woods *et al.* 2013; Hankin *et al.* 2011) using imaging mass spectrometry. However, while the above studies focused on changes on sphingolipids/ceramides, sulfatides, gangliosides, diacylglycerols and phospholipids which included PE, PI and PC, they did not evaluate the spatial distribution of CL. This information is important for the design and development of targeted therapies and evaluating their efficacy in TBI.

TBI occurs as a consequence of a direct mechanical impact, causing the brain to move rapidly within the cranium leading to tissue injury. As a consequence of membrane rupture at the site of impact and its immediate environment, there emerges an imbalance in the ionic

equilibrium on postsynaptic membranes altering fluxes of K^+, Na^+ and Ca^{2+} ions, complicated by the presynaptic release of neuro-transmitters and disorganized metabolic responses that may last from minutes to days (Prins *et al.* 2013; Werner *et al.* 2007). Changes in cerebral blood flow and intracranial pressure also contribute substantially to tissue damage from the initial trauma (Prins *et al.* 2013; Werner *et al.* 2007). Ineffective attempts by ionic pumps to reinstate the ionic homeostasis lead to ATP depletion causing an energy crisis, thus demanding increased respiration rates, and resulting in elevated rates of electron flow through mitochondrial complexes (Prins *et al.* 2013; Werner *et al.* 2007). This leads to increased production of reactive oxygen species contributing to further damage within mitochondria (Prins *et al.* 2013; Werner *et al.* 2007; Cheng *et al.* 2012).

Similar imbalances in ionic equilibrium, mitochondrial dysfunction and oxidative damage have been reported after cerebral ischemia (Bazan, 1992; Chen *et al.* 2011) and traumatic injury to spinal cord (Azbill *et al.* 1997; Sullivan *et al.* 2007; Stys *et al.* 1999; Obrenovitch *et al.* 1997). Indeed, reactive oxygen species (ROS), such as peroxynitrite and reactive aldehydes derived from the peroxidation of lipids, have been shown to be involved in the mitochondrial dysfunction associated with spinal cord injury (SCI) and TBI (Xiong *et al.* 2009; Vaishnav *et al.* 2010). As a result, numerous studies have demonstrated varying degrees of mitochondrial protection by scavenging lipid peroxyl radicals or using a variety of antioxidants and mitochondrial uncoupling agents (Mustafa *et al.* 2010; Patel *et al.* 2014; Bains *et al.* 2012; Patel *et al.* 2012; Patel *et al.* 2010; Patel *et al.* 2009; Mu *et al.* 2002; McEwen et al. 2007; Jin et al. 2004).

In response to various forms of cellular insults which result in mitochondrial dysfunction, cells attempt to eliminate their depolarized and damaged mitochondria by employing a specialized type of autophagy, namely mitophagy, - which, if successful, represents a rescue pathway (Kim *et al.* 2011). Mitophagic signaling engages specialized lipid signaling whereby a unique mitochondrial phospholipid, cardiolipin (CL, Ptd_2Gro), gets translocated to the surface of the outer membranes and acts as an “eat-me signal” (Chu *et al.* 2013). If mitophageal efforts are insufficient, the apoptotic program is activated to eradicate the cell. In this program, CL, more accurately its oxidation products, are involved as required executioners of the apoptotic program (Kagan *et al.* 2005). CL oxidation is catalyzed by an intermembrane space heme-protein, cytochrome c (cyt c). While cyt c normally acts as a shuttle of electrons between respiratory complexes III and IV, in depolarized mitochondria it switches to become a CL-specific peroxidase thus contributing to the production of a variety of oxygenated lipid mediators (Kagan *et al.* 2005; Tyurina *et al.* 2014). Thus, CLs are involved - as key signaling mechanisms - in responses of damaged neurons to mechanical trauma.

CLs (1,3-bis(sn-3′-phosphatidyl)-sn-glycerol) are structurally unusual anionic phospholipids as they contain two phosphatidyl groups (linked to a glycerol backbone) and four fatty acyl chains. In eukaryotic cells, mitochondrial CLs contain predominantly long carbon chains (from C16 to C22) that are polyunsaturated (from 2 to 6 double bonds). Importantly, these polyunsaturated fatty acids (PUFA) are readily oxidizable leading to the formation of numerous CL oxidation (CL-ox) products. CLs exist in low abundance compared to other phospholipids and are confined predominantly to the inner leaflet of the inner mitochondrial

membrane (IMM), yet they play a central role in the life and death of cells. They associate with various components of the electron transport chain and are critical for overall mitochondrial bioenergetic function and are also partially responsible for maintaining mitochondrial architecture, giving the IMM its characteristic high degree of curvature (Hoch 1992; Kagan *et al.* 2009; Claypool *et al.* 2011; Schlame 2008; Osman *et al.* 2011; Bazan *et al.* 2013; Winge 2012; Wirtz *et al.* 2011; Rosca *et al.* 2011). It is believed that these structural roles of CLs are fully met by the homo-acylated species of CLs, such as tetra-linoleoyl-CL, leading to its dominant presentation in mammalian tissues with high bioenergetic demands (e.g., heart, skeletal muscles) (Schlame *et al.* 1993). In contrast, high diversification is characteristic of tissues where the signaling functions of CLs are of critical importance culminating in more than 300 species in the brain (Ji *et al.* 2012; Bayir *et al.* 2007). This high degree of acyl chain diversification in CL was shown in an earlier report whereby SFAs, MUFAs, n-3 PUFAs and n-6 PUFAs represented 20.2, 25.6, 23.5 and 30.7 mol % of the fatty acyl chain composition of total brain CL in the mice, respectively (Ellis, *et al.* 2005). Interestingly, in mice lacking alpha-synuclein, CL's acyl chain composition was increased in SFA (51%) and decreased in n-6 PUFA (25 %, Ellis *et al.* 2005). These changes were accompanied by a decrease in linked complex I/III ETC activity with no changes in individual complex activities noted. These results further support the importance of brain CL acyl chain diversity in bioenergetics and signaling in normal and pathological states.

While the diversity of CL species has been firmly established for the whole brain, surprisingly, the distribution and abundance of different CL species in different anatomical areas of the brain and their vulnerability to TBI induced damage remain poorly characterized. This is mostly due to the low abundance of CL which is composed of multiple species. While our previous reports indicated that CL is selectively oxidized following TBI and presents itself as a target for the redox therapy of brain injury (Ji *et al.* 2012), the regional/spatial changes within damaged brain tissue with regard to this critical phospholipid remained undetermined. Here, we utilized our previously published protocol which employs a combination of enzymatic and chemical modifications on-tissue in conjunction with MALDI mass spectrometry (Amoscato *et al.* 2014; Sparvero *et al.* 2010; Sparvero *et al.* 2012) to allow for successful mass spectrometric imaging of CL in brain tissue from a controlled cortical impact (CCI) TBI model. We demonstrate, for the first time, dramatic decreases in CL content in the contusional (cortical) area as well as in hippocampal and thalamic regions that are further removed from the site of injury.

Materials and Methods

Reagents

Chloroform and ethanol (HPLC grade) were purchased from Sigma-Aldrich (St. Louis, MO, USA). Methanol was LC-MS grade from Fisher Scientific (Pittsburgh, PA, USA). 2-(4-Morpholino)ethane sulfonic acid (MES) was BioReagent grade also from Fisher Scientific (Pittsburgh PA, USA). Water was purified by a milliQ system (EMD Millipore, Billerica, MA, USA). 1-ethyl-3-[3-dimethylaminopropyl]carbodiimide hydrochloride (EDC) was purchased from Thermo Scientific/Pierce Biotechnology (Rockford, IL, USA).

Phospholipase C from *B. cerus,* ammonium acetate, and 2,5-dihydroxybenzoic acid (DHB) were also purchased from Sigma-Aldrich (St. Louis, MO, USA).

Animals and tissue preparation

All procedures were pre-approved and performed according to the protocols approved by the Institutional Animal Care and Use Committee of the University of Pittsburgh. TBI was induced by CCI to the left parietal cortex in three 17 day old male Sprague Dawley rats (Harlan, Indianapolis, IN, USA) as described previously (Ji *et al.* 2012). A metal pneumatically-driven 6 mm impactor tip was used (impact velocity 4.0 ± 0.2 m/s, penetration depth 2.5 mm). Three naive 17 day old male rats were used as controls. The brains were harvested 3 h after injury and immediately frozen in liquid nitrogen with neither fixation nor embedding, and stored at −80° C until sectioning. Brain tissue was affixed to a cryotome block with minimal Tissue-Tek OCT (Sakura FineTek USA, Torrance CA, USA). The blade and working surfaces of the cryotome were cleaned with methanol immediately prior to cutting, and at no time did the blade come into contact with the OCT. Consecutive 10 μm coronal brain sections were cut at −21 °C in the following order for: MALDI-IMS (1), H&E, MALDI-IMS (2), IHC, MALDI-IMS (3), lipid extraction. This sequence was repeated from Bregma −2.3 mm to Bregma −3.2 mm (Paxinos *et al.* 1982). Sections for MALDI-IMS were applied to cold histology slides coated with a conductive indium-tin oxide (ITO) surface (Delta Technologies LTD, Loveland, CO, USA) while other sections were applied to plain glass slides. This order allowed us to produce serial sections for ratiometric imaging of CL and semi-serial sections for H&E and the analysis of other lipid species. Lipid extraction from 5.0 mg of dried tissue sections on glass slides was performed using a modified Folch method as described previously (Folch *et al.* 1957). Total lipid extracts were dried under a steady stream of grade 5.0 N_2 then dissolved in 2:1 chloroform:methanol to a total volume of 200 μL and stored at −80 °C prior to use.

For CL imaging, the tissue was prepared as previously described (Amoscato *et al.* 2014). Briefly, the tissue was first treated with 500 mM EDC in MES buffer (100 mM, pH 3.7) for 2 h at room temperature then washed with 50 mM ammonium acetate buffer, pH 6.7 (200 μl per wash). The tissue was then treated with phospholipase C (0.005 units) for 15 min at 37 °C in ammonium acetate buffer (50 mM, pH 6.7). The tissue was then washed again with ammonium acetate buffer as described above. After the chemical/enzymatic treatments, the tissue was vacuum dried (2 h). 2,5-dihydroxybenzoic acid solution (DHB, Sigma-Aldrich, St. Louis, MO) was used as the matrix at 0.5 M in 2:1 chloroform:methanol with internal calibrants consisting of tetramyristoylcardiolipin (TMCL) and sphingomyelin(d18:1/12:0, Avanti Polar Lipids, Alabaster, AL, USA) at 5 and 20 μM, respectively. The matrix was applied using an aerosol device constructed in-house (Amoscato *et al.* 2014) and housed in a PCR chamber (Coy Laboratories, Michigan, USA) inside a fume hood in order to minimize variability from airflow cross-currents. The nozzle height was 120 mm with a spray time of 10 min without interruption at a flow rate of 2400 μL/h.

Mass Spectrometry Analysis

MALDI time-of-flight (TOF) -MS and –IMS (imaging mass spectrometry) analyses were performed using an ABI 4800 mass spectrometer equipped with an N_2 laser (AB Sciex,

Framingham, MA, USA). ITO slides were fitted to the MALDI target with an AB 4800 Slide Glass Guide for 2 pieces (Hudson Surface Technology, Old Tappan, NJ). All imaging was performed at a 200 μm lateral resolution with random walking every 50 laser shots. Using the instrument control software (AB Sciex, Framingham, MA, USA) the laser attenuations value was set to 6100 arbitrary units. Three hundred shots were acquired per imaging location except for reflector-positive mode which used 100 shots. The mass analysis range was *m/z* 400 to 2000 in reflector-positive mode and 700 to 2000 in reflector-negative mode. For MS1 imaging, three tissue sections were imaged from each animal (two untreated analyzed with reflector positive and negative modes and one treated with EDC-PLC analyzed with reflector negative mode). The negative-mode MS/MS imaging was performed on two additional EDC/PLC-treated sections from two out of the three animals and the mass windows were centered on the cardiolipin clusters at *m/z* 1448 (72-carbon CL) and 1476 (74-carbon CL) and was set at 20 Th to allow only species from that particular cluster. A grid of 200 μm coordinate locations covering the entire tissue section was generated on an Excel worksheet and imported into the MALDI control software as a custom plate type and spot set. Spatial locations for MALDI-IMS were determined by co-registering fiducials on optical images acquired from a microscope prior to matrix deposition. This spot set was run in batch mode to generate an array of t2d spectrum files. These files were converted to mzXML format using the t2d converter (downloaded from www.pepchem.org/download/converter.html) that uses OpenMS tools (Sturm *et al.* 2008). The data conversion requires Microsoft Windows 7 (www.microsoft.com) and Oracle Java (www.java.com). These mzXML files were then converted to mzML format with ProteoWizard (Chambers *et al.* 2012). A datacube in imzML format (Schramm *et al.* 2012) was then generated from these individual mzML files with imzML Converter (Race *et al.* 2012). Finally, the MALDI images were generated from the imzML datacube with MSI Reader v0.06 (Robichaud *et al.* 2013) using the following settings: TIC normalization, zero-order interpolation, intensity summing at 0.5 Da windows centered on the exact mass, jet heatmap. For a detailed explanation regarding spectra acquisition and data conversion for .td2 files on the ABI-4800 MALDI instrument, see supplementary methods.

MALDI-MS Data Analysis

Images are displayed as ion spatial distributions with intensities relative to the given ion (0% to 100% for all images). Using H&E stained semi-serial sections and a rat brain atlas (Paxinos *et al.* 1982) as a guide, areas around anatomical regions of interest (ROIs) were drawn and the intensity information for given *m/z* values was exported into a spreadsheet using the “ROI Selection” and “Export Intensity Data” tools in MSI Reader. Since the size of the anatomical regions varied slightly between different animals, the total number of pixels from the ROIs for each animal varied. Average intensities of an ion within a given anatomical ROI were calculated and compared as ipsilateral/contralateral ratios (for CCI) or left/right ratios (for naive) from the same brain section. Each paired set of ion intensity ratios from a brain section’s ROI was imported into its own spreadsheet. These ratios were compiled into naive and CCI-TBI groups. Three CCI animals and three naive animals were used for determining ratios and a two-tailed t-test was performed to determine significance of difference between these two groups for the ratios of the same ion. A one-way ANOVA (SPSS, IBM) was performed to determine if a significant difference existed in CL loss

between different molecular species within each CCI-TBI ROI. In order to determine which molecular species of CL showed significant differences in the amount of ipsi-/contralateral loss as compared to other CL species, Tukey's post hoc test (SPSS, IBM) was performed between different molecular species within each CCI-TBI ROI.

Immunohistochemistry (IHC)

The slides for IHC were stored at −20 °C until they were ready to be stained. Sections were rehydrated with approximately 500 μL of phosphate buffered saline (1x PBS). Chemical fixation in 2 % paraformadehyde (PFA) occurred at room temperature (approximately 18–19 °C) for 20 minutes. The samples were then washed with approximately 1 mL of 1x PBS. Tissue permeabilization was accomplished via 0.1 % Trition (Sigma, Triton X-100, Cat. #: T-9184) detergent at room temperature for 15 minutes. Samples were washed with 1 mL of 0.5 % bovine serum albumin (BSA) (Sigma-Aldrich, bovine serum albumin-lyophilized, Cat. #: A4503-50G). Arbitrary binding of secondary antibodies was blocked using 20 % normal goat serum (Sigma-Aldrich, Sera from Normal Goat, Cat. #: G9023-5ML) at room temperature for 45 minutes. Samples were washed with 1 mL of 0.5 % BSA. Primary antibody, TOM20 (Santa Cruz, Host- Rabbit, Cat. #: sc-11415, working concentration 5 μg/mL) was diluted (1:100) in 0.5% BSA followed by incubation at room temperature for 1 hour. The samples were then thoroughly washed with a volume of 3 mL of 0.5 % BSA. Incubation with secondary antibodies goat-anti-mouse Cy3 (Jackson ImmunoResearch, Cat. #: 115-165-166, working concentration 2 μg/mL) and goat-anti-rabbit Alexa Fluor 488 (Molecular Probes, Cat. #: A-11034, working concentration 2 μg/mL) diluted (1:1000 and 1:500 respectively) in 0.5 % BSA followed, at room temperature for 1 hour. The samples were then thoroughly washed with a volume of 3 mL of 1x PBS. Hoechst nuclear stain (Invitrogen, Cat. #: H3570, working concentration 10 μg/mL) was added to the samples and incubated at room temperature for 30–45 seconds. The samples were then washed with 1 mL of 1x PBS. Gelvatol mounting media was prepared according to a standard protocol (www.cbi.pitt.edu) and this was used to mount a cover glass to the slide.

Ratiometric Imaging

Sections for ratiometric imaging were labelled with antibodies to TOM 20 (cat. # sc-11415/A3113, Santa Cruz Biotechnology, Inc., Dallas, TX), nuclei counter stained with Hoescht dye and mounted as previously described (Amoscato *et al.* 2014). Entire sections were scanned and images collected using a Nikon 90i (Melville, NY, USA) upright microscope, 20x dry plan apochromat objective and motorized stage. Individual images were stitched together using Nikon Elements software. To overlay the MALDI-IMS data with the immunocytochemical data fiduciary structures common to the semi-serial IMS and light microscopy images were identified. The MALDI-IMS images were resized such that the pixel count matched that of the light microscopy images and images combined into a single file. Various additive combinations of the MALDI-IMS images were made and rendered to the same bit depth (12 bit) as the light microscopy images and ratios calculated of MALDI-IMS intensity/mitochondrial label intensity generated. These images are displayed as monochrome images with a ratio between 0 and 50.

Statistical analysis

Data are expressed as mean ± S.D. as indicated in the figure legends. Changes in ipsi/contralateral signal intensities for given ion intensities for control and CCI tissue were analyzed by a two-tailed Student's t-test. In addition, CL ion intensities were analyzed by a 1-way ANOVA (SPSS, IBM) and Tukey's post hoc test (SPSS, IBM) for comparisons. Differences were considered significant at $p < 0.05$.

Results

CL molecular species demonstrate regional specificity in the brain

Our MALDI imaging protocol resolved 23 isobaric species of CLs in the brain of control animals (Fig. 1a and 1b). The most abundant signals (CL species containing 72, 74 and 76 carbons) corresponded to CLs containing at least one or more arachidonic acid (AA) fatty acyl chain. A number of the CL clusters had intensities sufficient for fragmentation analysis indicating that the majority of the individual molecular forms were represented by PUFA-CLs, which were thus more abundant than non-oxidizable saturated and mono-unsaturated CLs (see Fig. 1b (top panel) and Supplementary Table 1). These MALDI data were independently confirmed by LC-MS/MS analysis (Fig. 1c). As in our MALDI-IMS analysis, our LC-MS analysis indicated a diverse speciation with the CL clusters containing 72 and 74 acyl carbons (CL 72:X, CL 74:X) as the prominent clusters (~25% each of total CL). This was followed by CL 76:X (~20%) and CL 70:X (~11%). Additional minor CL clusters accounted for the remaining percentage (78:X (~7%), CL 80:X (~7%), CL 68:X (~3%), not shown). Our further detailed MS/MS fragmentation analysis indicated that all possible CL species (to approximately 94%) have at least one or more PUFA in their structure which was in line with previously published data (see Supplementary Table 1, Amoscato *et al.* 2014; Bayir *et al.* 2007; Ji *et al.* 2012). Interestingly, this was dissimilar to CLs in many other mammalian tissues where linoleic acid-containing CL species dominate (Schlame 2008; Schlame *et al.* 1993).

Further, we comparatively analyzed the CL speciation in four different anatomical regions of the brain (Fig. 1b). Overall we found that signal intensities corresponding to concentrations of some of the CL species varied in different anatomical areas of the brain. This resulted in different "biochemical" maps of individual CLs for the respective areas (for example, compare heat map of CL (70:4) to that of CL (76:12) in Fig. 1a). This also was reflected in the intensities of MALDI signals for these respective species collected from representative areas from each anatomical region as shown in Fig. 1b. For example, the signal intensity of the CL (70:4) species was highest in the hippocampal area as compared to the cortex and thalamus and is reflected in the accompanying heat maps. Moreover, these specific spectra displayed differences from the MALDI spectra collected from the entire brain. Figure 1d displays a naive H&E stained optical image with enlargements of representative areas. In the context of TBI induced oxidative stress, these data indicate that the areas with higher levels of PUFA CLs may be more vulnerable to oxidative modifications.

TBI results in decreases in cardiolipin molecular species at the site of injury and in the hippocampal and thalamic regions of the brain

CLs were severely decreased in the ipsilateral (impacted) side of the brain as compared to the contralateral side. This was most evident in the tissue immediately below the impact region where all CL species are decreased (compare Figs. 1a and 2a). Intensity ratios for the CCI (ipsilateral/contralateral) and naive (left/right) samples are shown in Supplementary Table 2. Ratios approaching unity indicate no change between regions whereas ratios less than unity indicate a decrease in CL intensity between these regions within the same tissue section.

Comparison of the intensity ratios from CCI tissue sections to naive tissue sections at the same Bregma showed that each of the CL species were significantly lower in the injured region assessed at 3 h post injury (as compared to the identical contralateral region) and lower as compared to the same CL species from the naive brain tissue sections ($p<0.05$). Ranges for the CL ratios for the CCI vs. naive contusional region (see Supplementary Table 2) were as follows: CL, 70 carbon cluster, 0.78–0.81 vs. 1.02–1.04; CL, 72 carbon cluster, 0.59–0.73 vs. 1.08–1.10; CL, 74 carbon cluster, 0.46–0.60 vs. 1.05–1.13; CL, 76 carbon cluster, 0.50–0.65 vs. 1.07–1.1. We also noted a “gradient” effect with regard to the CL species that were affected with the greater decreases associated with the more polyunsaturated CL species (Fig. 3a). This is clearly seen in the negative slope associated with the ipsilateral side of the CCI cortex tissue (contusional) versus the near-zero slope of the adjacent (non-contusional) cortex (Fig. 4 **(panels a and b)**).

We have extended our findings further to include ipsilateral/contralateral comparisons of three additional regions: 1) a cortical region adjacent to the area of impact; 2) the hippocampus and 3) the thalamic region. Comparison of an adjacent cortical region to the area of impact to an identical contralateral region indicated that CL intensity ratios remained unchanged (i.e. ratios approaching unity, Figs. 2a, 3b and **Table 2**). In addition, no significant CL changes were noted comparing this area to an identical area on a naive tissue section of the same Bregma (Supplementary Table 2).

Interestingly, areas distant to the site of impact, such as the hippocampal and the thalamic regions, also suffered significant decreases ($p < 0.05$) in CL signals on the ipsilateral side as compared to the contralateral side (**compare** Figs. 1a and 2a) although no histological evidence of damage was noted (Fig 2b). These results indicate that MSI is able to detect early CL alterations when histology cannot. Comparing the hippocampal CL ratios for t5he CCI vs. naive tissue sections, the ranges (Supplementary Table 2) were as follows: CL, 70 carbon cluster, 0.86–0.88 vs. 1.00–1.01; CL, 72 carbon cluster, 0.75–0.88 vs. 1.00–1.05; CL, 74 carbon cluster, 0.65–0.79 vs. 1.00–1.05; CL, 76 carbon cluster, 0.68–0.78 vs. 1.00–1.03. Likewise, the decreases in thalamic CL ratios for the CCI vs. naive tissue sections were all significant ($p < 0.05$) and yielded the following results: CL, 70 carbon cluster, 0.88–0.90 vs. 0.98–1.00; CL, 72 carbon cluster, 0.83–0.87 vs. 0.98–1.02; CL, 74 carbon cluster, 0.74–0.88 vs. 0.98–1.00; CL, 76 carbon cluster, 0.70–0.80 vs. 0.95–0.98 (Figs. 1a and 2, Fig. 3 c and d). Here again, a “gradient” effect was observed: polyunsaturated CLs were affected more severely than CLs containing saturated (SFA) and monounsaturated (MUFA) fatty acids in

both the hippocampal and thalamic areas (Figure 4, c and d). A comparison of p-values for individual CL species in CCI tissue is shown in Supplementary Figure 1.

The decreases seen in CL species on the ipsilateral side at the site of impact, in an adjacent cortical region as well as in the hippocampal and thalamic regions are further supported by MS/MS data on CL clusters (Fig. 5b and d). MS/MS analysis of the remaining 72:X and 74:X CL clusters on the ipsilateral side of the CCI tissue indicated, as expected, decreases in CL product ions which included 16:0 (*m/z* 255.2), 16:1 (*m/z* 253.2), 18:0 (*m/z* 283.2), 18:1 (*m/z* 281.2), 18:2 (*m/z* 279.2), 20:4 (*m/z* 303.2), 22:6 (*m/z* 327.2) fatty acyl chains as well as intermediate phosphatidic acid (PA, *m/z* 719.5, 699.5, 697.5 and 695.5) and lysoPA-H_2O (*m/z* 439.2, 417.2, 415.2 and 389.2) fragment ions. These changes were not evident in the naive samples (Fig. 5a and c).

MALDI imaging results for other phospholipid species in the impact region, adjacent cortex, hippocampal and thalamic regions

Phosphatidylinositol species (PI, *m/z* 883.5 and 885.5) displayed a significant ($P < 0.05$) decrease in ipsilateral/contralateral ratios in CCI tissue sections at the point of impact (Fig. 6 and Supplementary Table 2) similar to that described for CL (intensity ratio range for PI, 0.36–0.44 vs. 1.0–1.1). Naive tissues sections showed no such changes. A significant decrease ($p < 0.05$) was noted for PI species *m/z* 885.5 in the hippocampus (intensity ratio range for CCI vs. naive 0.72–0.83 vs. 0.96–1.05) while a significant decrease ($p < 0.05$) in PI *m/z* 883.5 species was noted in the thalamus (intensity ratio range for CCI vs. naive 0.85–0.91 vs. 0.98–1.03). Neither of these decreases were as robust as that seen for CLs. No significant changes in PI intensity were noted in regions adjacent to the area of impact.

The major sulfatide species (*m/z* 806.6, 888.6 and 906.6, Fig. 6 and Supplementary Table 2), which are not normally abundant outside the white matter, displayed no noticeable changes (ipsilateral/contralateral) in the thalamic and hippocampal regions in the CCI tissue sections. The major gangliosides displayed only a decrease at the point of impact (Supplementary Fig. 2), with ipsilateral/contralateral ratios below unity in some of the tissue sections (see Supplementary Table 2 for individual ipsilateral/contralateral ratios). No other noticeable changes were evident for ganglioside species in the hippocampal, thalamic and adjacent cortex regions.

Overall, these results indicate that the associated changes in intensities of the various lipids in the CCI model are not a generalized global effect on all lipids; rather, they are lipid and regio-specific. Moreover, CLs displayed the most pronounced TBI induced regio-specific changes not only in the zone of immediate impact (cortex) but in other anatomical areas – the hippocampal and thalamic ipsilateral regions of the brain.

Ratiometric analysis of CL to mitochondria confirms CL loss in the cortex contusional area as well as the hippocampus and thalamus

To confirm that the loss of CL signal in the CCI-TBI model was a result of insult rather than a change in the relative distribution of individual CLs in mitochondria among various anatomical areas of the brain, we performed ratiometric analysis of CL images relative to mitochondrial abundance using immunohistochemical (IHC) imaging of mitochondria from

semi-serial sections. Ratiometric images in naive rat brain tissue correlated very well with our imaging mass spectrometry data, displaying little to no change in the cortex contusional area (a), a cortical region adjacent to the contusional area (b), the hippocampus (c) and thalamus (d) among the various CL species (Supplementary Fig. 3). In contrast, ratiometric images of CL in the CCI-TBI tissues displayed lower CL/mitochondrial ratios in the cortex contusional area (a), hippocampus (c) and thalamus (d), indicating less CL signal as compared to the mitochondrial IHC signal on the ipsilateral (damaged) side of the brain (Supplementary Fig. 4). CL/mitochondrial ratios on the contralateral side remained unchanged in these areas, confirming our finding that in the CCI-TBI model, CL loss extends into the hippocampal and thalamic areas on the ipsilateral side of the brain.

Discussion

This work presents, for the first time, a “biochemical map” of individual molecular species of CLs and their distribution in several anatomical regions of normal and acutely injured brain. Two major mitochondrial functions of CLs, i) structural in bioenergetics and ii) signaling in coordinating metabolism - may be fulfilled by different molecular forms of CLs – homoacylated (mostly, tetralinoleoyl-CLs) and hetero-acylated (CLs containing highly PUFA residues such as AA, EPA, DHA) (Tyurina *et al.* 2014; Schlame *et al.* 1993). The latter is achieved by using CLs as a mitochondrial source of oxygenated lipid mediators generated via peroxidation of CLs by cyt c and subsequent hydrolysis of its oxidation products by Ca^{2+}-independent PLA_2 (Tyurina *et al.* 2014). This pathway is a Ca^{2+}-independent alternative to a conventional mechanism of the production of lipid mediators via the sequential action of Ca^{2+}-dependent PLA2 and oxygenation of the released free PUFA by lipoxygenase/cyclooxygenase-driven enzymatic reactions.

Acute brain injury, chronic neurodegenerative diseases, as well as spinal cord injury have been known to rely on lipid mediators, such as eicosanoids and docosanoids, as potent regulators of inflammatory responses. Eicosanoids generated through the enzymatic oxidation of AA via cyclooxygenases, lipoxygenases and epoxygenases have potent effects on cell death, inflammation and the immune response (O’Banion 1999; Vane *et al.* 1998; Phillis *et al.* 2006; Kuhn *et al.* 2006; Kin *et al.* 2008; Spector *et al.* 2009; Murphy et al 1994; Saunders *et al.* 1987). In particular, AA and DHA are released mainly by cytosolic phospholipase A_2 or plasmalogen-selective phospholipase A_2, respectively (Farooqui *et al.* 2000; Hirashima *et al.* 1992; Farooqui 2010, Demediuk *et al.* 1985; Saunders *et al.* 1987). Free AA is either incorporated into phospholipids by re-acylation or oxidized by enzymatic/non-enzymatic mechanisms producing a variety of signaling mediators involved in gene transcription, inflammation, oxidative stress and neurodegeneration (Farooqui *et al.* 2000; Lee *et al.* 2004; Rapoport 1999; Wolfe *et al.* 1994; Murphy *et al.* 1994; Saunders *et al.* 1987). On the other hand, DHA is converted into resolvins and neuroprotectins via 15-LOX-like enzymes (Hong et al. 2003; Marcheselli et al. 2003). While the mechanisms of formation of a variety of the AA and DHA precursors are known, their phospholipid precursors as well as the subcellular sites from which they originated (cytosolic vs. mitochondrial or other organelles) are less clear. With regard to the current study, we report a loss of CL in the contusion which in part may be due to physical damage. In addition, we also suggest that, in the response to mechanical trauma, CL loss in the cortex and more

importantly in the hippocampus and thalamus, may be a result of hydrolysis of various CL precursors for further downstream signaling events.

Traditionally, previous studies in the area of TBI have demonstrated a critical decrease in energy to the affected tissue, resulting in decreased amounts of ATP production allowing for an increased production of oxidative free radicals within mitochondria (Robertson *et al.* 2006; Robertson *et al.* 2007; Robertson *et al.* 2004; Lifshitz *et al.* 2004; Lifshitz *et al.* 2003; Singh *et al.* 2006). The resulting energy crisis has been supported by subsequent studies demonstrating decreases in a variety of mitochondrial enzymatic activities which ultimately affect the overall structure and function of mitochondria.

Mitochondrial fate after TBI has been studied by several groups and their results paint a clear picture of mitochondrial biochemical demise. Robertson, et al. reported a decrease in the pyruvate dehydrogenase complex activity as well as a decrease in cytochrome c content on the damaged (ipsilateral) side of rat brains at 4 h post TBI in a CCI model (Robertson *et al.* 2006; Robertson *et al.* 2007; Robertson *et al.* 2004). These findings were supported by other groups which demonstrated decreases in respiratory control ratios at 3 h post TBI with subsequent increases in reactive oxygen species (ROS) and ultrastructural alterations in mitochondria which included swelling, disrupted cristae and outer mitochondrial membrane (OMM) rupture (Robertson *et al.* 2007; Lifshitz *et al.* 2003; Lifshitz *et al.* 2004). As expected, less mitochondrial protein was present in the contusional area as compared to the corresponding contralateral area (Lifshitz *et al.* 2004; Lifshitz *et al.* 2003). While the hippocampal mitochondrial protein levels remained unchanged between ipsilateral (impacted) and contralateral sides of the brain tissue, ATP levels declined significantly in the ipsilateral hippocampus (Lifshitz *et al.* 2004; Lifshitz *et al.* 2003). A portion of these hippocampal mitochondria appeared to sustain damage, exhibiting swelling, ballooned membranes and a reduced mitochondrial permeability transition pore (mPTP) sensitivity to Ca^{2+} (Prins *et al.* 2013; Werner *et al.* 2007; Lifshitz *et al.* 2004; Lifshitz *et al.* 2003). Indeed, many forms of TBI result in increased levels of Ca^{2+}, with excessive mitochondrial sequestration of this cation ultimately leading to the opening of the mPTP, swelling and eventual OMM rupture and loss of cyt c (Robertson *et al.* 2004).

Since mechanical trauma has been associated with a decrease in ATP production, this will more than likely affect acyl chain turnover in the brain. Acyl-CoA dependent remodeling is a highly energy dependent process whereby approximately 25–30% of this tissue's energy expenditure is utilized for the maintenance of this biochemical process (Contreras *et al.* 2000; Igarashi *et al.* 2007; Rapoport 2001; Rapoport *et al.* 2001; DeMar *et al.* 2004; Lee *et al.* 2005; Rapoport 2008). In addition to acyl chain turnover, increased energy expenditure may also be necessary for downstream lipid signaling (Lukiw *et al.* 2008; Chen *et al.* 2005; Bazan 2005). Indeed, energy expenditure is necessary for mitochondrial and cellular bioenergetics, metabolism and signaling (Mejia *et al.* 2014; Mejia *et al.* 2016; Mejia *et al.* 2015; Mejia *et al.* 2014; Mitchell *et al.* 2009; Taylor *et al.* 2009; Taylor *et al.* 2012; Xu *et al.* 2010) which are comprised of a number of specific and irreversible chemical reactions. However, CL remodeling by tafazzin is both non-specific and reversible, producing only a minimal drop in free energy making this reaction essentially energy independent (Schlame *et al.* 2013). In addition, the literature indicates that the turnover of CL is slower than that of

other phospholipids (Xu *et al.* 2014) such that substantial loss due to turnover within a 3 h post-CCI time period would be unlikely. Thus, the loss in CL as reported in this study may be the prelude to decreased ATP production ultimately affecting overall lipid biosynthesis and remodeling at later time points.

Herein, we have described a mass spectrometric imaging study which investigated the changes in the critical mitochondrial phospholipid, CL, in a CCI model of TBI. With CL's intimate connection to mitochondrial bioenergetics, physiology and structure, we provide evidence, for the first time, of regio-specific CL changes. Significant CL decreases occurred not only within the contusional area, but extended well beyond the area of impact into the hippocampus and thalamus following CCI. Phosphatidylinositol displayed significant decreases, although its changes in the hippocampal and thalamic regions were not as dramatic as compared to CL. Remarkably, signals for gangliosides, sulfatides, PC and SM remained essentially unchanged in the hippocampal and thalamic regions. Since our CL imaging protocol did not involve scanning in the *m/z* range below 400 to avoid potential low mass matrix clusters and utilized PLC and EDC treatment of the tissue for CL visualization, we cannot rule out changes in cholesterol or plasmalogen species in response to TBI at later time points. Imaging of phosphatidylcholine (PC) and sphingomyelin (SM) lipids in positive mode provided two intriguing findings. First, sodium adducts of PC displayed an increase in the area of impact whereas potassium adducts of the same PC species displayed a concomitant decrease (data not shown). The same held true for the SM species. These changes in the cortical impact area are in agreement with a previous study whereby changes in PC adduct formation were noted in a mass spectrometric imaging study (Hankin et al. 2011). These findings most likely reflect neuronal depolarization and the resultant disrupted ionic equilibrium that occurs on the postsynaptic membranes in the contusional area, which drastically influences Na^+, K^+ and Ca^{2+} fluxes, likely causing a redistribution of lipid adduct ions.

Previous mass spectrometric imaging studies have provided essential information on the spatial distribution of various (non-cardiolipin) lipid species in response to blast injury and ischemia/reperfusion injury (Woods *et al.* 2013; Hankin *et al.* 2011). In the study assessing lipid changes in response to blast induced "mild" TBI, major increases in ganglioside GM2 were noted in the hippocampus, thalamus and hypothalamus after a single blast exposure (Woods *et al.* 2013). Changes were seen as early as 2 h. On the other hand, a concomitant decrease in ceramides was also noted in the same study. Mass spectrometric imaging studies by Hankin et al. demonstrated changes in lysophosphatidylcholine, PC, PE and SM that were specific to their adduct ions in response to ischemia/reperfusion injury in the brain (Hankin *et al.* 2011). In an elegant study by Roux, et al. (Roux *et al.* 2016) the authors utilized an implanted silver nanoparticle protocol to image rat brain lipids over time in a CCI model of TBI (Roux, *et al.* 2015, in press). While CL was not assessed by this method and longer time points post-TBI were chosen (1,3 and 7 days), their results indicated that increases in SM and ceramide were noted as early as one day post-TBI in the injured cortex. Their region of interest was defined by pixels that differed significantly from control when comparing the same lipid species. This region of interest included the cortical impact site and regions immediately adjacent to this. In addition, changes in diacylglycerols (increases in 6 species), cholesteryl esters (increases in 8 species), PE (decreases in 3 species), PI

(decrease/increase in one species) and sulfatides (decrease, one species) were noted at later time points (day 3 and 7 post-TBI). Thus, losses in CL at the 3 h time point as determined in this study may constitute an early response mechanism to TBI.

One possibility for the loss in CL and PI signals could be related to their potential for lipid oxidation in the presence of mitochondrial ROS generated following TBI due to the overall high degree of unsaturation present in their fatty acyl chains. This characteristic of CL and PI lipid species make them extremely susceptible to ROS attack and potential degradation. However, in this scenario, one would also expect other unsaturated lipid species to be prone to signal loss, however, this was not observed. While oxidation/degradation may contribute in part to loss of signal, cleavage of potential oxygenated PUFAs of CL, as potential mitochondrial lipid signals in response to TBI, may also be involved. Such a role for the generation of novel CL signals in mitochondria has already been reported in a cyt *c*/H_2O_2 model system (Tyurina *et al.* 2014). In this study, it was demonstrated that by using brain CLs, a significant variety of lipid mediators could be generated by the cyt *c*-catalyzed oxygenation process. Specifically, eight well known linoleic acid-based and nine AA-based lipid mediators were generated by cyt *c*/H_2O_2 from brain CL's. In a similar manner, PI loss, (via head group modification and cleavage), having already been established as a traditional signaling cascade, may contribute to lower intensities of this lipid in the CCI model system. Indeed, several studies have demonstrated the critical role of the PI3K/Akt signaling pathway as a cell survival mechanism that is activated in the injured brain after TBI (Brazil *et al.* 2002; Iadecola *et al.* 2011; Chen *et al.* 2012). Thus, degradation of CL and PI via oxidation and specific cleavage of the oxidatively-derived products functioning as upstream signaling molecules (either as damage sensors and/or as self-protective signals promoting neuronal survival) may both contribute to the overall loss of these lipid species as assessed by MS imaging in a CCI-TBI model system.

In conclusion, we have demonstrated, for the first time, regional/spatial CL decreases not only within the contusional area but in the hippocampal and thalamic regions, distant from the site of injury in an established and well characterized CCI model system of TBI. The decreases are not a generalized effect on all lipids; rather, they are confined predominantly to CL and PI. The specific decreases in CL, which ultimately will affect electron transport chain (ETC) function and mitochondrial architecture, are most likely key effectors of the decrease in various ETC enzymatic activities, the loss of cytochrome c, and the decrease in ATP production. While degradation of CL and PI via oxidation of their polyunsaturated fatty acyl chains by ROS may contribute to their subsequent loss, cleavage of these oxidized lipids as potential sources of lipid mediators should also be considered as an additional underlying mechanism that is activated as a self-protective/signaling response to traumatic brain injury. Future improved technologies will afford better resolved spatial resolution along with direct detection of oxygenated CL species and their signaling products.

Supplementary Material

Refer to Web version on PubMed Central for supplementary material.

Acknowledgments

Supported by NIH: ES020693, U19AIO68021, NS076511, NS061817; NIOSH OH008282; U54 GM103529 08 (SCW); partial support from Fulbright Canada (VEK); WH81XWH-10-1-0623 and WH81XWH-14-2-0018 (PMK). This project used the UPCI Cancer Biomarkers Facility that is supported in part by award P30CA047904.

Abbreviations

TBI	traumatic brain injury
CL	cardiolipin
MALDI	matrix-assisted laser desorption/ionization
MALDI-MS	MALDI mass spectrometry
PUFA	polyunsaturated fatty acids
MUFA	monounsaturated fatty acids
SFA	saturated fatty acids
CCI	controlled cortical impact
LC-MS	liquid chromatography-mass spectrometry
MES	2-(4-Morpholino)ethane sulfonic acid
EDC	1-ethyl-3-[3-dimethylaminopropyl]carbodiimide hydrochloride
DHB	2,5-dihydroxybenzoic acid
ITO	indium-tin oxide
TMCL	tetramyristoylcardiolipin
TOF	time-of-flight
IHC	immunohistochemistry
IMS	imaging mass spectrometry
PFA	paraformaldehyde
BSA	bovine serum albumin
PC	phosphatidylcholine
PE	phosphatidylethanolamine
SM	sphingomyelin
MS/MS	tandem mass spectrometry (fragmentation analysis)
PI	phosphatidylinositol
PA	phosphatidic acid

AA	arachidonic acid
EPA	eicosapentaenoic acid
DHA	docosahexaenoic acid
LOX	lipoxygenase
COX	cyclooxygenase
ROS	reactive oxygen species
OMM	outer mitochondrial membrane
mPTP	mitochondrial permeability transition pore
PI3K	phosphatidylinositol-3-kinase
CL-ox	cardiolipin oxidation
LC-MS	liquid chromatography-mass spectrometry
cyt c	cytochrome c
IMM	inner mitochondrial membrane
SCI	spinal cord injury
DHA	docosahexaenoic acid

References

Amoscato AA, Sparvero LJ, He RR, Watkins S, Bayir H, Kagan VE. Imaging mass spectrometry of diversified cardiolipin molecular species in the brain. Anal Chem. 2014; 86:6587–95. [PubMed: 24949523]

Azbill RD, Mu X, Bruce-Keller AJ, Mattson MP, Springer JE. Impaired mitochondrial function, oxidative stress and altered antioxidant enzyme activities following traumatic spinal cord injury. Brain Res. 1997; 765:283–90. [PubMed: 9313901]

Bains M, Hall ED. 2) Antioxidant therapies in traumatic brain and spinal cord injury. Biochim Biophys Acta. 9201; 1822:675–84. [PubMed: 22080976]

Bayir H, Tyurin VA, Tyurina YY, Viner R, Ritov V, Amoscato AA, Zhao Q, Zhang XJ, Janesko-Feldman KL, Alexander H, Basova LV, Clark RS, Kochanek PM, Kagan VE. Selective early cardiolipin peroxidation after traumatic brain injury: an oxidative lipidomics analysis. Ann Neurol. 2007; 62:154–69. [PubMed: 17685468]

Bazan, NG. Modulators of neural cell signaling and triggering of gene expression following cerebral ischemia. In: Ischen, NG.Braquet, P., Ginsberg, MD., editors. Advances in Neurochemistry. Vol. 7. Plenum Press; New York: 1992. p. 321-333.

Bazan NG. Lipid signaling in neural plasticity, brain repair and neuroprotection. Mol Neurobiol. 2005; 32:89–103. [PubMed: 16077186]

Bazan NG. The onset of brain injury and neurodegeneration triggers the synthesis of docosanoid neuroprotective signaling. Cell Mol Neurobiol. 2006; 26:901–913. [PubMed: 16897369]

Bazan S, Mileykovskaya E, Mallampalli VKPS, Heacock P, Sparagna GC, Dowhan W. Cardiolipin-dependent reconstitution of respiratory supercomplexes from purified Saccharomyces cerevisiae complexes III and IV. J Biol Chem. 2013; 288:401–411. [PubMed: 23172229]

Brazil DP, Park J, Hemmings BA. PKB binding proteins. Getting in on the Akt Cell. 2002; 111:293–303. [PubMed: 12419241]

Centers for Disease Control & Prevention. CDC grand rounds. Reducing severe traumatic brain injury in the United States. MMWR. Morbidity and mortality weekly report. 2013; 62:549–552. [PubMed: 23842444]

Chambers MC, MacLean B, Burke R, Amode D, Ruderman DL, Neumann S, Gatto L, Fischer B, Pratt B, Egertson J, Hoff K, Kessner D, Tasman N, Shulman N, Frewen B, Baker TA, Brusniak MY, Paulse C, Creasy D, Flashner L, Kani K, Moulding C, Seymour SL, Nuwaysir LM, Lefebvre B, Kuhlmann F, Roark J, Rainer P, Detlev S, Hemenway T, Huhmer A, Langridge J, Connolly B, Chadick T, Holly K, Eckels J, Deutsch EW, Moritz RL, Katz JE, Agus DB, MacCoss M, Tabb DL, Mallick P. A cross-platform toolkit for mass spectrometry and proteomics. Nat Biotech. 2012; 30:918–920.

Chen C, Bazan NG. 5) Lipid signaling: sleep synaptic plasticity and neuroprotection. Prostaglandins and other lipid mediators. 9200; 77:65–76.

Chen H, Yoshioka H, Kim GS, Jung JE, Okami N, Sakata H, Maier CM, Narasimhan P, Goeders CE, Chan PH. Oxidative stress in ischemic brain damage: mechanisms of cell death and potential molecular targets for neuroprotection. Antioxid Redox Signal. 2011; 14:1505–1517. [PubMed: 20812869]

Chen SF, Tsai HJ, Hung TH, Chen CC, Lee CY, Wu CH, Wang PY, Liao NC. Salidroside improves behavioral and histological outcomes and reduces apoptosis via PI3K/Akt signaling after experimental traumatic brain injury. PLoS One. 2012; 7:e45763. [PubMed: 23029230]

Cheng G, Kong R, Zhang L, Zhang J. Mitochondria in traumatic brain injury and mitochondrial-targeted multipotential therapeutic strategies. Br J Pharmacol. 2012; 167:699–719. [PubMed: 23003569]

Chu CT, Ji J, Dagda RK, Jiang J, Tyurina YY, Kapralov AA, Tyurin VA, Yanamala N, Shrivastava IH, Mohammadyani D, Wang KZK, Zhu J, Klein-Seetharaman J, Balasubramanian K, Amoscato AA, Borisenko G, Huang Z, Gusdon AM, Cheikhi A, Steer EK, Wang R, Baty C, Watkins S, Bahar I, Bayir H, Kagan VE. Cardiolipin externalization to the outer mitochondrial membrane acts as an elimination signal for mitophagy in neuronal cells. Nat Cell Biol. 2013; 15:1197–1205. [PubMed: 24036476]

Claypool SM, Koehler CM. The complexity of cardiolipin in health and disease. Trends in Biomed Sci. 2011; 37:32–41.

Colicos MA, Dixon CE, Dash PK. Delayed, selective neuronal death following experimental cortical impact injury in rats: possible role in memory deficits. Brain Res. 1996; 739:111–119. [PubMed: 8955931]

Contreras MA, Greiner RS, Chang MC, Myers CS, Salem N, Rapoport SI. Nutritional deprivation of alpha-linoleic acid decreases but does not abolish turnover and availability of unacylated docoahexaenoic acid and docosahexaenoyl-CoA in rat brain. J Neurochem. 2000; 75:2392–400. [PubMed: 11080190]

DeMar JC Jr, Ma K, Bell JM, Rapoport SI. Half-lives of docosahexaenoic acid in rat brain phospholipids are prolonged by 15 weeks of nutritional deprivation of n-3 polyunsaturated fatty acids. J Neurochem. 2004; 91:1125–37. [PubMed: 15569256]

Demediuk P, Saunders RD, Anderson DK, Means ED, Horrocks LA. Membrane Lipid Changes in Laminectomized and Traumatized Cat Spinal Cord. PNAS. 1985; 82:7071–7075. [PubMed: 3863139]

Ellis CE, Murphy EJ, Mitchell DC, Golovko MY, Scaglia F, Barcelo-Coblijn GC, Nussbaum RL. Mitochondrial lipid abnormality and electron transport chain impairment in mice lacking alpha-synuclein. Mol Cell Biol. 2005; 25:10190–10201. [PubMed: 16260631]

Farooqui AA. Studies on plasmalogen-selective PLA_2 in brain. Mol Neurobiol. 2010; 41:267–273. [PubMed: 20049656]

Farooqui AA, Ong WY, Horrocks LA, Farooqui T. Brain cytosolic phospholipase A_2: Localization, role and involvement in neurological diseases. Neuroscientist. 2000; 6:169–180.

Faul, M., Xu, L., Wald, MM., Coronado, VG. National Center for Injury Prevention and Control Centers for Disease Control and Prevention. Atlanta, GA: 2010.

Folch J, Lees M, Sloane Stanley GH. A simple method for the isolation and purification of total lipides from animal tissues. J Biol Chem. 1957; 226:497–509. [PubMed: 13428781]

Geddes DM, LaPlaca MC, Cargill RS 2nd. Susceptibility of hippocampal neurons to mechanically induced injury. Exp Neurol. 2003; 184:420–427. [PubMed: 14637111]

Hall ED, Vaishnav RA, Mustafa AG. Antioxidant therapies for traumatic brain injury. Neurotherapeutics. 2010; 7:51–61. [PubMed: 20129497]

Hankin JA, Farias SE, Barkley RM, Heidenreich K, Frey LC, Hamazaki K, Kim HY, Murphy RC. MALDI mass spectrometric imaging of lipids in rat brain injury models. J Am Soc Mass Spectrom. 2011; 22:1014–1021. [PubMed: 21953042]

Hirashima Y, Farooqui AA, Mills JS, Horrocks LA. Identification and purification of calcium-independent phospholipase A_2 from bovine brain cytosol. J Neurochem. 1992; 59:708–714. [PubMed: 1629740]

Hoch FL. Cardiolipins and biomembrane function. Biochim Biophys Acta. 1992; 1113:71–133. [PubMed: 1550861]

Hong S, Gronert K, devchaud PR, Moussignac RL, Serhan CN. 3) Novel docosatrienes and 17S-resolvins generated from docoshexaenoic acid in murine brain, human blood, and glial cells-Autacoids in anti-inflammation. J Biol Chem. 9200; 278:14677–14687. [PubMed: 12590139]

Iadecola C, Anrather J. Stroke research at a crossroad: asking the brain for directions. Nat Neurosci. 2011; 14:1363–1368. [PubMed: 22030546]

Igarashi M, DeMar JC Jr, Ma K, Chang L, Bell JM, Rapoport SI. Upregulated liver conversion of alpha-linolenic acid to docosahexaenoic acid in rats on a 15 week n-3 PUFA-deficient diet. J Lipid Res. 2007; 48:152–64. [PubMed: 17050905]

Ji J, Kline AE, Amoscato A, Samhan-Arias AK, Sparvero LJ, Tyurin VA, Tyurina YY, Fink B, Manole MD, Puccio AM, Okonkwo DO, Cheng JP, Alexander H, Clark RS, Kochanek PM, Wipf P, Kagan VE, Bayır H. Lipidomics identifies cardiolipin oxidation as a mitochondrial target for redox therapy of brain injury. Nat Neruosci. 2012; 15:1407–1413.

Jin Y, McEwen ML, Nottingham SA, Maragos WF, Dragicevic NB, Sullivan PG, Springer JE. The mitochondrial uncoupling agent 2,4-dinitrophenol improves mitochondrial function, attenuates oxidative damage and increases white matter sparing in the contused spinal cord. J Neurotrauma. 2004; 21:1396–404. [PubMed: 15672630]

Kagan VE, Tyurin VA, Jiang J, Tyurina YY, Ritov VB, Amoscato AA, Osipov AN, Belikova NA, Kapralov AA, Kini V, Vlasova II, Zhao Q, Zou M, Di P, Svistunenko DA, Kurnikov IV, Borisenko GG. Cytochrome c acts as a cardiolipin oxygenase required for release of proapoptotic factors. Nature chemical biology. 2005; 1:223–32. [PubMed: 16408039]

Kagan VE, Bayir HA, Belikova NA, Kapralov O, Tyurina YY, Tyurin VA, Jiang J, Stoyanovsky DA, Wipf P, Kochanek PM, Greenberger JS, Pitt B, Shvedov AA, Borisenko G. Cytochrome c/cardiolipin relations in mitochondria: a kiss of death. Free Rad Biol Med. 2009; 46:1439–1453. [PubMed: 19285551]

Kim C, Kim JY, Kim JH. cytosolic phospholipase A2, lipoxygenase metabolites and reactive oxygen species. BMB Rep. 2008; 41:555–559. [PubMed: 18755069]

Kim I, Lemasters JJ. Mitophagy selectively degrades individual damaged mitochondria after photoirradiation. Antioxid Redox Signal. 2011; 14:1919–1928. [PubMed: 21126216]

Kuhn H, O'Donnell VB. Inflammation and immune regulation by 12/15-lipoxygenases. Prog Lipid Res. 2006; 45:334–356. [PubMed: 16678271]

Lee HJ, Rao JS, Chang L, Rapoport SI, Bazinet RP. Chronic N-methyl-D-aspartate administration increases the turnover of arachidonic acid within brain phospholipids of the unanesthetized rat. J Lipid Res. 2008; 49:162–8. [PubMed: 17957090]

Lee H, Villacreses NE, Rapoport SI, Rosenberger TA. In vivo imaging detects a transient increase in brain arachidonic acid metabolism: a potential marker of neuroinflammation. J Neurochem. 2004; 91:936–945. [PubMed: 15525347]

Lewen A, Matz P, Chan PH. Free radical pathways in CNS injury. J Neurotrauma. 2000; 17:871–890. [PubMed: 11063054]

Lifshitz J, Friberg H, Neumar RW, Raghupathi R, Welsh FA, Janmey P, Saatman KE, Weiloch T. Structural and functional damage sustained by mitochondria after traumatic brain injury in the rat:

Evidence for differentially sensitive populations in the cortex and hippocampus. J Cerebral Blood Flow Met. 2003; 23:219–231.

Lifshitz J, Sullivan PG, Hovda DA, Weiloch T, McIntosh TK. Mitochondrial damage and dysfunction in traumatic brain injury. Mitochondrion. 2004; 4:705–713. [PubMed: 16120426]

Lukiw WJ, Bazan NG. Docosahexaenoic acid and the aging brain. J Nutrition. 2008; 138:2510–14. [PubMed: 19022980]

Marcheselli VL, Hong S, Lukiw WJ, tian XH, Gronert K, Musto A, Hardy M, Gimenez JM, Chiang N, Serhan CN, Bazan NG. 3) Novel docosanoids inhibit brain ischemia-reperfusion-mdeiated leukocyte infiltration and pro-inflammatory gene expression. J Biol Chem. 9200; 278:43807–43817. [PubMed: 12923200]

McEwen ML, Sullivan PG, Rabchevsky AG, Springer JE. targeting mitochondrial for the treatment of acute spinal cord injury. Neurotherapeutics. 2011; 8:168–179. [PubMed: 21360236]

McEwen ML, Sullivan PG, Springer JE. Pretreatment with the cyclosporine derivative, NIM811, improves the function of synaptic mitochondria following spinal cord contusion in rats. J Neurotrauma. 2007; 24:613–24. [PubMed: 17439345]

Mejia EM, Cole LK, Hatch GM. Mitochondrial metabolism and the role it plays in Heart failure and mitochondrial supercomplex formation. Cadiovasc Hematol Disord Drug Targets. 2014; 14:98–106.

Mejia EM, Hatch GM. Mitochondrial phospholipids: role in mitochondrial function. J Bioenerg Biomembr. 2016; 48:99–112. [PubMed: 25627476]

Mejia EM, Ibdah JA, Sparagna GC, Hatch GM. Differention reduction in cardiac and liver monolysocardiolipin acyltransferase-1 and reduction in cardiac and liver tetralinoleoyl-cardiolipin in the alpha-subunit of trifunctional protein heterozygous knockout mice. Biochem J. 2015; 47:123–9.

Mejia EM, Nguyen H, Hatch GM. Mammalian cardiolipin biosynthesis. Chem Phys Lipids. 2014; 179:11–16. [PubMed: 24144810]

Mitchell RW, Hatch GM. Regulation of cardiolipin biosynthesis by fatty acid transport protein-1 in HEK 293 cells. Biochim Biophys Acta. 2009; 1788:2015–21. [PubMed: 19523918]

Mu X, Azbill RD, Springer JE. NBQX treatment improves mitochondrial function and reduces oxidative events after spinal cord injury. J Neurotrauma. 2002; 19:917–27. [PubMed: 12225652]

Murphy EJ, Behrmann D, Bates CM, Horrocks LA. Lipid alterations following impact spinal cord injury in the rat. Mol Chem Neuropathology. 1994; 23:13–26.

Mussack T, Biberthaler P, Kanz KG, Wiedemann E, Gippner-Steppert C, Mutschler W, Jochum M. Serum S-100B and interleukin-8 as predictive markers for comparative neurologic outcome analysis of patients after cardiac arrest and severe traumatic brain injury. Crit Care Med. 2002; 30:2669–2674. [PubMed: 12483057]

Mustafa AG, Singh IN, Wang J, Carrico KM, Hall ED. Mitochondrial protection after traumatic brain injury by scavenging lipid peroxyl radicals. J Neurochem. 2010; 114:271–80. [PubMed: 20403083]

O'Banion MK. Cyclooxygenase-2: molecular biology, pharmacology and neurobiology. Crit Rev Neurobiol. 1999; 13:45–82. [PubMed: 10223523]

Obrenovitch TP, Urenjak J. Is high extracellular glutamate the key to excitotoxicity in traumatic brain injury? J Neurotrauma. 1997; 14:677–698. [PubMed: 9383088]

Osman C, Velker DR, Langer T. Making heads or tails of phospholipids in mitochondria. J Cell Biol. 2011; 192:7–16. [PubMed: 21220505]

Patel SP, Sullivan PG, Lyttle TS, Magnuson DS, Rabchevsky AG. Acetyl-L- carnitine treatment following spinal cord injury improves mitochondrial function correlated with remarkable tissue sparing and functional recovery. Neurosci. 2012; 210:296–307.

Patel SP, Sullivan PG, Lyttle TS, Rablchevsky AG. Acetyl-L-carnitine ameliorates mitochondrial dysfunction following contusion spinal cord injury. J Neurochem. 2010; 114:291–301. [PubMed: 20438613]

Patel SP, Sullivan PG, Pandya JD, Goldstein GA, VanRooyen JL, Yonutas HM, Eldahan KC, Morehouse J, Magnuson DS, Rabchevsky AG. N-acetylcysteine amide preserves mitochondrial

bioenergetics and improves functional recovery following spinal trauma. Exp Neurol. 2014; 257:95–105. [PubMed: 24805071]

Patel SP, Sullivan PG, Pandya JD, Rabchevsky AG. Differential effects of the mitochondrial uncoupling agent, 2,4-dinitrophenol, or the nitroxide antioxidant, Tempol, on synaptic or nonsynaptic mitochondria after spinal cord injury. J Neurosci Res. 2009; 87:130–40. [PubMed: 18709657]

Paxinos, G., Watson, C. The Rat Brain in Sterotaxic Coordinates. Academic Press; San Diego, California, USA: 1982.

Phillis JW, Horrocks LA, Farooqui AA. Cyclooxygenases, lipoxygenases and epoxygenases in CNS: their role and involvement in neurological disorders. Brain Res Rev. 2006; 52:201–243. [PubMed: 16647138]

Prins M, Greco T, Alexander D, Giza CC. The pathophysiology of traumatic brain injury. Disease Models & Mechanisms. 2013; 6:1307–1315. [PubMed: 24046353]

Race AM, Styles IB, Bunch J. Inclusive sharing of mass spectrometry imaging data requires a converter for all. J Proteomics. 2012; 75:5111–5112. [PubMed: 22641155]

Rapoport SI. In vivo fatty acid incorporation into brain phospholipids in relation to signal transduction and membrane remodeling. Neurochem res. 1999; 24:1403–1415. [PubMed: 10555781]

Rapoport SI. In vivo fatty acid incorporation into brain phosholipids in relation to plasma availability, signal transduction and membrane remodeling. J Mol Neurosci. 2001; 16:243–61. [PubMed: 11478380]

Rapoport SI. Arachidonic acid and the brain. J Nutrition. 2008; 138:2515–2520. [PubMed: 19022981]

Rapoport SI, Chang MC, Spector AA. Delivery and turnover of plasma derived essential PUFAs in mammalian brain. J Lipid Res. 2002; 42:678–85.

Robertson CL, Bucci CJ, Fiskum G. Mitochondrial response to calcium in the developing brain. Brain Res Dev Brain Res. 2004; 151:141–148. [PubMed: 15246700]

Robertson CL, Saraswati M, Fiskum G. Mitochondrial dysfunction early after traumatic brain injury in immature rats. J Neurochem. 2007; 101:1248–1257. [PubMed: 17403141]

Robertson CL, Soane L, Siegel ZT, Fiskum G. The potential role of mitochondria in pediatric traumatic brain injury. Dev Neurosci. 2006; 28:432–446. [PubMed: 16943666]

Robichaud G, Garrard KP, Barry JA, Muddiman DC. MSiReader: An Open-Source Interface to View and Analyze High Resolving Power MS Imaging Files on Matlab Platform. J Am Soc Mass Spectrom. 2013; 24:718–721. [PubMed: 23536269]

Rosca M, Minkler P, Hoppel CL. Cardiac mitochondria in heart failure: normal cardiolipin profile and increased threonine phosphorylation of complex IV. Biochim Biophys Acta. 2011; 1807:1373–82. [PubMed: 21320465]

Roux A, Muller L, Jackson SN, Post J, Baldwin K, Hoffer B, Balaban CD, Barbacci D, Schultz JA, Gouty S, Cox BM, Woods AS. Mass spectrometry imaging of rat brain lipid profile changes over time following traumatic brain injury. J Neurosci Meth. (in press).

Sato M, Chang E, Igarashi T, Noble LJ. Neuronal injury and loss after traumatic brain injury: time course and regional variability. Brain Res. 2001; 917:45–54. [PubMed: 11602228]

Saunders RD, Dugan LL, Demediuk P, Means ED, Horrocks LA, Anderson DK. Effects of methylprednisolone and the combination of alpha-tocopherol and selenium on arachidonic acid metabolism and lipid peroxidation in traumatized spinal cord tissue. J Neurochem. 1987; 49:24–31. [PubMed: 3108455]

Schlame M. Cardiolipin synthesis for the assembly of bacterial and mitochondrial membranes. J Lipid Res. 2008; 49:1607–1620. [PubMed: 18077827]

Schlame M. Cardiolipin remodeling and the function of tafazzin. Biochim Et Biophys Acta. 2013; 1831:582–588.

Schlame M, Brody S, Hostetler KY. Mitochondrial cardiolipin in diverse eukaryotes. Eur J Biochem. 1993; 212:727–733. [PubMed: 8385010]

Schramm T, Hester A, Klinkert I, Both J-P, Heeren RMA, Brunelle A, Laprévote O, Desbenoit N, Robbe M-F, Stoeckli M, Spengler B, Römpp A. imzML — A common data format for the flexible exchange and processing of mass spectrometry imaging data. Journal of Proteomics. 2012; 75(16): 5106–5110. [PubMed: 22842151]

Singh IN, Sullivan PG, Deng Y, Mbye LH, Hall ED. Time course of post-traumatic mitochondrial oxidative damage and dysfunction in a mouse model of focal traumatic brain injury: implications for neuroprotective therapy. J Cerebral Blood Flow & Metab. 2006; 26:1–12.

Sparvero LJ, Amoscato AA, Dixon CE, Long JB, Kochanek PM, Pitt BR, Bayir H, Kagan VE. Mapping of phospholipids by MALDI imaging (MALDI-MSI): realities and expectations. Chem Phys Lipids. 2012; 165:545–62. [PubMed: 22692104]

Sparvero LJ, Amoscato AA, Kochanek PM, Pitt BR, Kagan VE, Bayir H. Mass-spectrometry based oxidative lipidomics and lipid imaging: applications in traumatic brain injury. J Neurochem. 2010; 115:1322–36. [PubMed: 20950335]

Spector AA. Arachidonic acid cytochrome P450 epoxygenase pathway. J Lipid Res. 2009; 50(Suppl):S52–S56. [PubMed: 18952572]

Sturm M, Bertsch A, Gröpl C, Hildebrandt A, Hussong R, Lange E, Pfeifer N, Schulz-Trieglaff O, Zerck A, Reinert K, Kohlbacher O. OpenMS – an Open-Source Software Framework for Mass Spectrometry. BMC Bioinformatics. 2008; 9:163.doi: 10.1186/1471-2105-9-163 [PubMed: 18366760]

Stys PK, Li S. At physiological temperature, Na-Ca exchange plays an important role in mediating spinal cord white matter injury. J Neurotrauma. 1999; 16:984.

Sullivan PG, Krishnamurthy S, Patel SP, Pandya JD, Rabchevsky AG. Temporal characterization of mitochondrial bioenergetics after spinal cord injury. J Neurotrauma. 2007; 24:991–9. [PubMed: 17600515]

Tang YP, Noda Y, Hasegawa T, Nabeshima T. A concussive-like brain injury model in mice (II): selective neuronal loss in the cortex and hippocampus. J Neurotrauma. 1997; 14:863–873. [PubMed: 9421457]

Taylor WA, Harch GM. Identification of the human mitochondrial linoleoyl-Coenzyme A monolysocardiolipin acyltransferase (MLCL At-1). J Biol Chem. 2009; 284:30360–71. [PubMed: 19737925]

Taylor WA, Majia EM, Mitchell RW, Choy PC, Sparagna GC, Hatch GM. Human trifunctional protein alpha links cardiolipin remodeling to beta-oxidation. PLoS One. 2012; 7:e48628. [PubMed: 23152787]

Tyurina YY, Poloyac SM, Tyurin VA, Kapralov AA, Jiang J, Anthonymuthu TS, Kapralova VI, Vikulina AS, Jung MY, Epperly MW, Mohammadyani D, Klein-Seetharaman J, Jackson TC, Kochanek PM, Pitt BR, Greenberger JS, Vladimirov YA, Bayır H, Kagan VE. A mitochondrial pathway for biosynthesis of lipid mediators. Nat Chem. 2014; 26:1407–1418.

Vaishnav RA, Singh IN, Miller DM, Hall ED. Lipid peroxidation-derived reactive aldehydes directly and differentially impair spinal cord and brain mitochondrial function. J Neurotrauma. 2010; 27:1311–20. [PubMed: 20392143]

Vane JR, Bakhle YS, Botting RM. Cyclooxygenases 1 and 2. Annu Rev Pharmacol Toxicol. 1998; 38:97–120. [PubMed: 9597150]

Werner C, Engelhard K. Pathophysiology of traumatic brain injury. Br J Anaesthesia. 2007; 99:4–9.

Winge DR. Sealing the mitochondrial respirasome. Mol Cell Biol. 2012; 32:2647–52. [PubMed: 22586278]

Wirtz S, Schuelke M. Region-specific expression of mitochondrial complex I genes during murine brain development. PLoS One. 2011; 6:1–12.

Woods AS, Colsch B, Jackson SN, Post J, Baldwin K, Roux A, Hoffer B, Cox BM, Hoffer M, Rubovitch V, Pick CG, Schultz JA, Balabon C. Gangliosides and ceramide change in a mouse model of blast induced traumatic brain injury. ACS Chem Neurosci. 2013; 4:594–600. [PubMed: 23590251]

Xiong Y, Hall ED. Pharmacological evidence for a role of peroxynitrite in the pathophysiology of spinal cord injury. Exp Neurol. 2009; 216:105–14. [PubMed: 19111721]

Xu FY, McBride H, Acehan D, Vaz FM, Houtkooper RH, Lee RM, Mowat MA, Hatch GM. The dynamics of cardiolipin synthesis post-mitochondrial fusion. Biochim Biophys Acta. 2010; 1798:1577–85. [PubMed: 20434430]

Xu Y, Schlame M. The turnover of glycerol and acyl moieties of cardiolipin. Chem Phys Lipids. 2014; 179:17–24. [PubMed: 24184572]

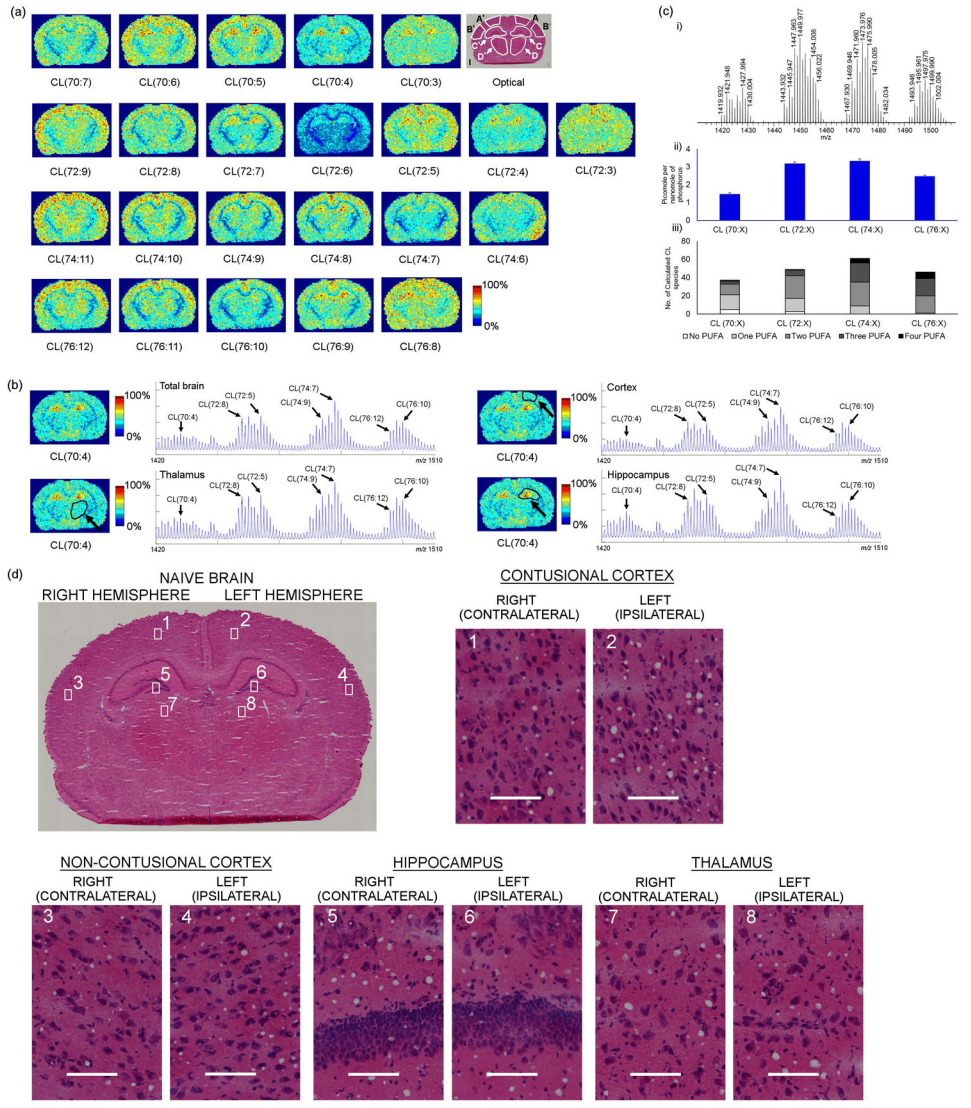

Fig. 1. MALDI-MS images and representative spectra of CL in naive rat brain tissue

(a): IMS negative ion mode heat maps of CL $[M-H]^-$ species from an entire naive rat brain coronal section (spatial resolution, 200 microns) treated with EDC-PLC (representative images from 3 animals). Individual images for CL species include CL clusters 70:X, 72:X, 74:X and 76:X indicating the total number of fatty acyl carbons (70, 72, 74 or 76) and the total number of double bonds (:X). A corresponding H&E optical image (scale bar = 1 mm) is shown with regions of interest including (A,A′) the left/right contusional region, (cortex); (B,B′) an adjacent non-contusional region, (cortex); (C,C′) the left/right hippocampus and (D,D′) the left/right thalamus, respectively. MALDI-MS images are displayed as relative intensities with respect to the given CL species. **(b)**: Representative average CL $[M-H]^-$ spectra from total brain (intensity averaged from 2615 pixels), and ipsilateral thalamus (156 pixels), contusional cortex (89 pixels) and hippocampus (124 pixels). Representative heat maps for the CL (70:4) species for the different anatomical areas are shown as relative intensities with the region indicated. **(c)**: (i) CL $[M-H]^-$ spectrum from LC-MS analysis of rat brain cortex assessed within the same mass range as that presented for MALDI-IMS; (ii)

quantitation of CL clusters and (iii) a stacked histogram representing the number of possible CL species in each cluster containing zero, one, two, three and four PUFA in their acyl chains. **(d)**: H&E 4X optical image with zoom-in of representative regions at 10X including (1,2) right/left contusional cortex; (3,4) right/left non-contusional cortex; (5,6) right/left hippocampus and (7,8) right/left thalamus, respectively. White scale bar = 100 microns.

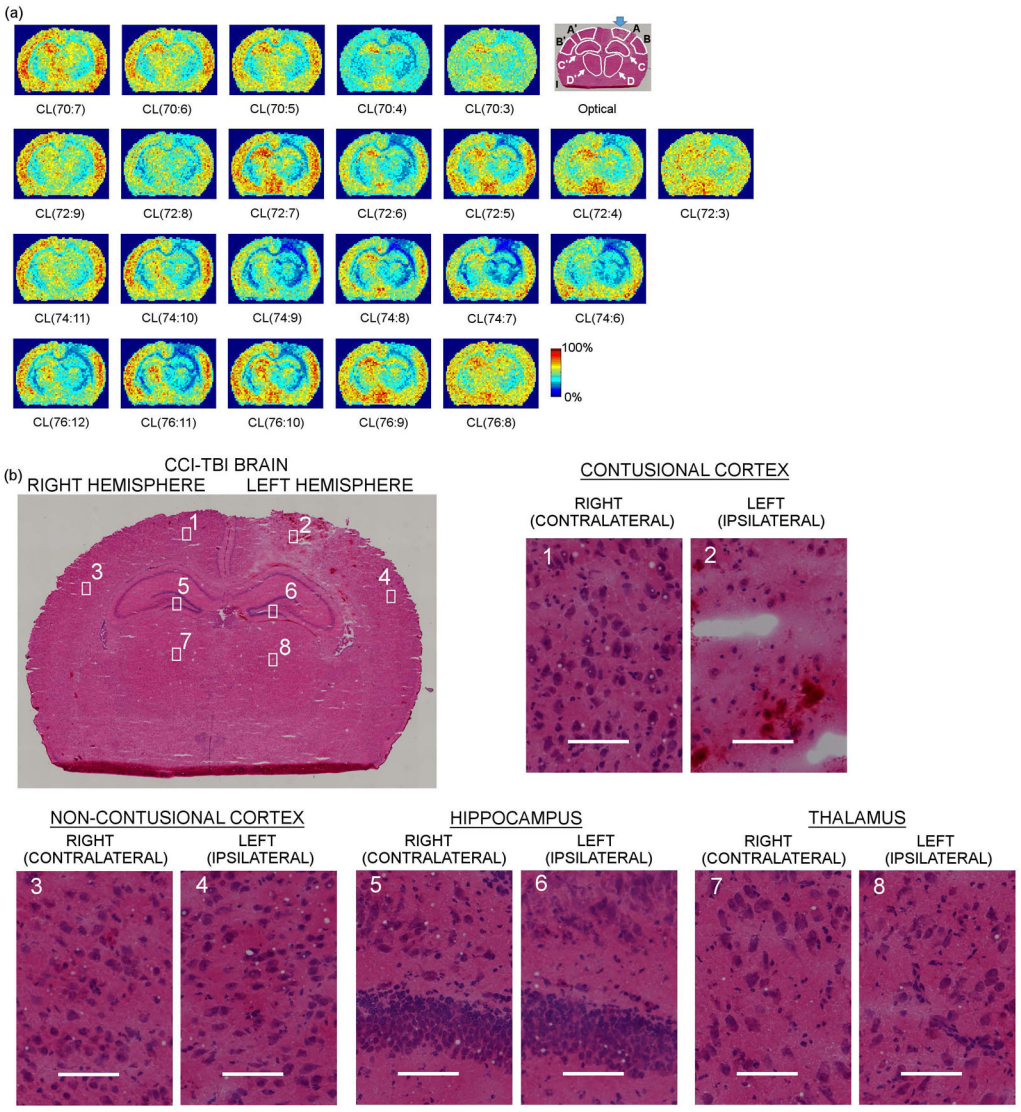

Fig. 2. MALDI-MS images of CL in CCI rat brain tissue

(a). IMS negative ion mode heat maps of CL $[M-H]^-$ species from an entire CCI rat brain coronal section (spatial resolution, 200 microns) treated with EDC-PLC (representative images from 3 animals). Individual images for CL species include CL clusters 70:X, 72:X, 74:X and 76:X indicating the total number of fatty acyl carbons (70, 72, 74 or 76) and the total number of double bonds (:X). A corresponding H&E optical image (scale bar = 1 mm) is shown with regions of interest including (A,A′) the ipsi/contralateral (right/left) contusional region, (cortex); (B,B′) an adjacent non-contusional region, (cortex); (C,C′) the ipsi/contralateral hippocampus and (D,D′) the ipsi/contralateral thalamus, respectively. The large blue arrow indicates the point of impact for the CCI tissue section. MALDI-MS images are displayed as relative intensities. **(b)**: H&E 4X optical image with zoom-in of representative regions at 10X including (1,2) contra/ipsilateral contusional cortex; (3,4) contra/ipsilateral non-contusional cortex; (5,6) contra/ipsilateral hippocampus and (7,8) contra/ipsilateral thalamus, respectively. White scale bar = 100 microns.

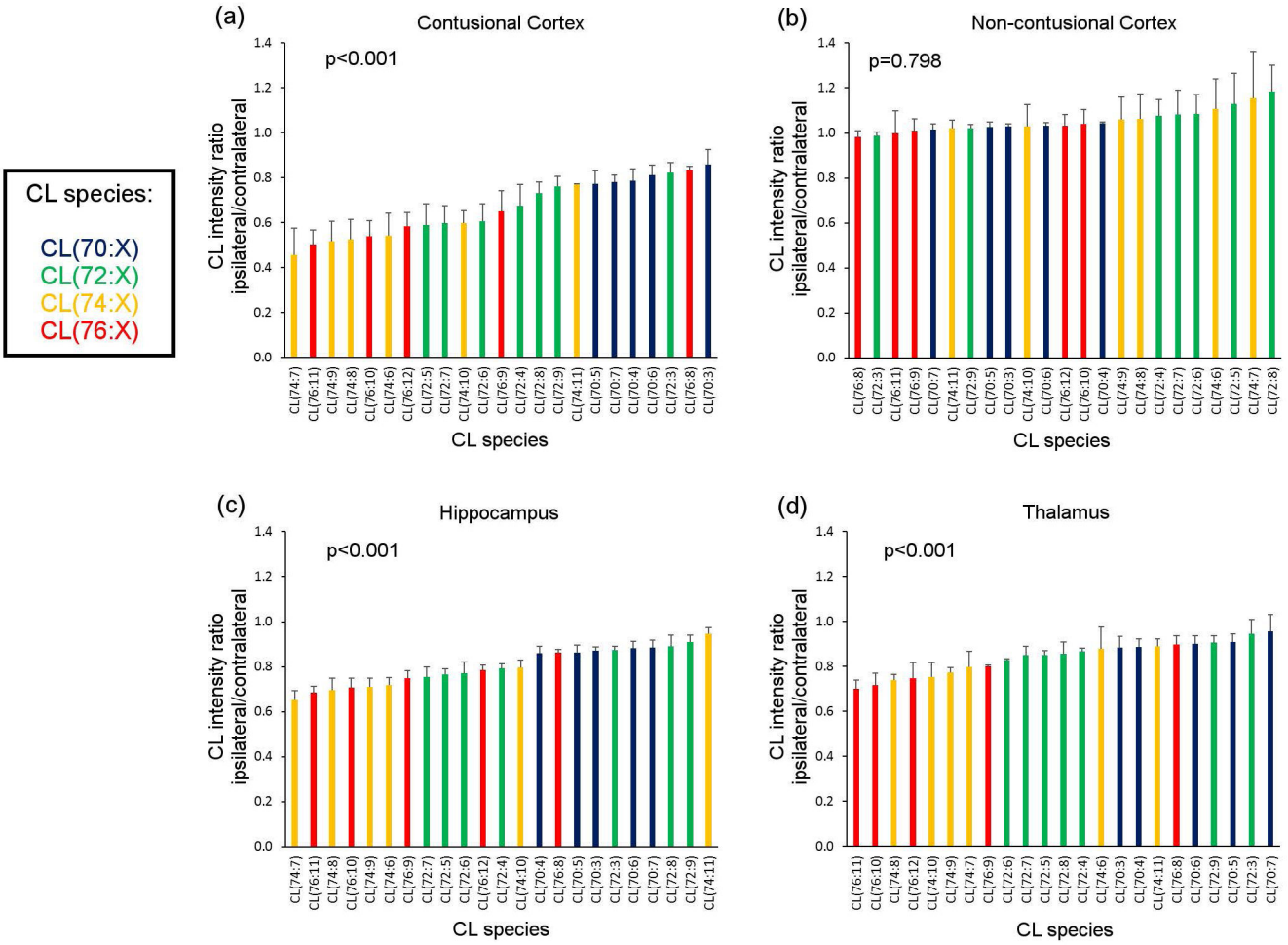

Fig. 3. Species-specific CL loss in the ipsilateral cortex, hippocampus and thalamus in response to CCI

Average CL signals from areas on the ipsilateral side of a CCI-TBI section were divided by the average intensity of the same ion on an identical area on the contralateral side for the **a**) contusional area (intensity averaged from 89 pixels per side), **b**) an adjacent non-contusional area of the cortex (89 pixels), **c**) hippocampus (124 pixels) and **d**) thalamus (156 pixels). Ratios of CL signals were plotted for individual CL $[M-H]^-$ species ordered from the species most affected (i.e. greatest loss) to the species least affected (least loss). Ratios approaching unity indicate little to no loss. CL clusters containing 76 carbons (red), 74 carbons (yellow), 72 carbons (green) and 70 carbons (blue) are shown. One-way ANOVA determined that the between-groups p-value for different CL species was <0.001 for each ROI except for the non-contusional cortex.

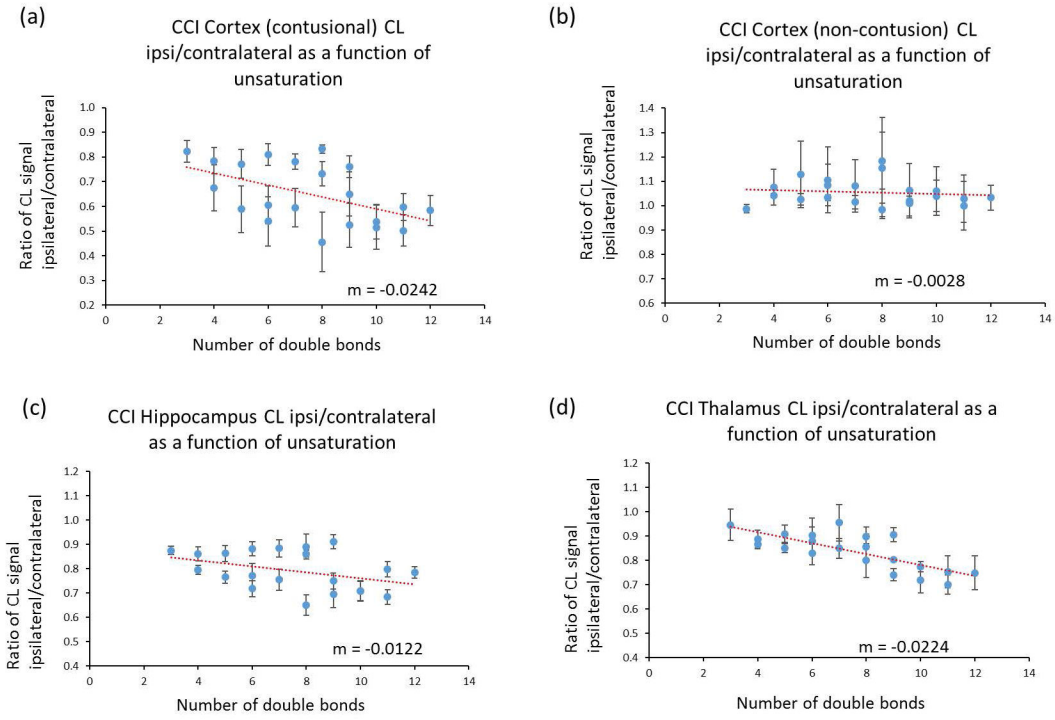

Fig. 4. Trend line analysis comparing the loss of CL signal in CCI tissue with the degree of CL unsaturation in various brain regions

Ipsilateral to contralateral ratios of CL signals were plotted vs. number of double bonds contained in the CL species for the **a**) cortex contusional area, **b**) an adjacent non-contusional area of the cortex, **c**) hippocampus and **d**) thalamus. A trend line was generated for each of the four brain areas above. Slopes (m) appear at the bottom of each graph. Panels a, c and d display negative slopes indicating a greater loss of CL signal with an increasing degree of unsaturation. Panel b displays little to no change.

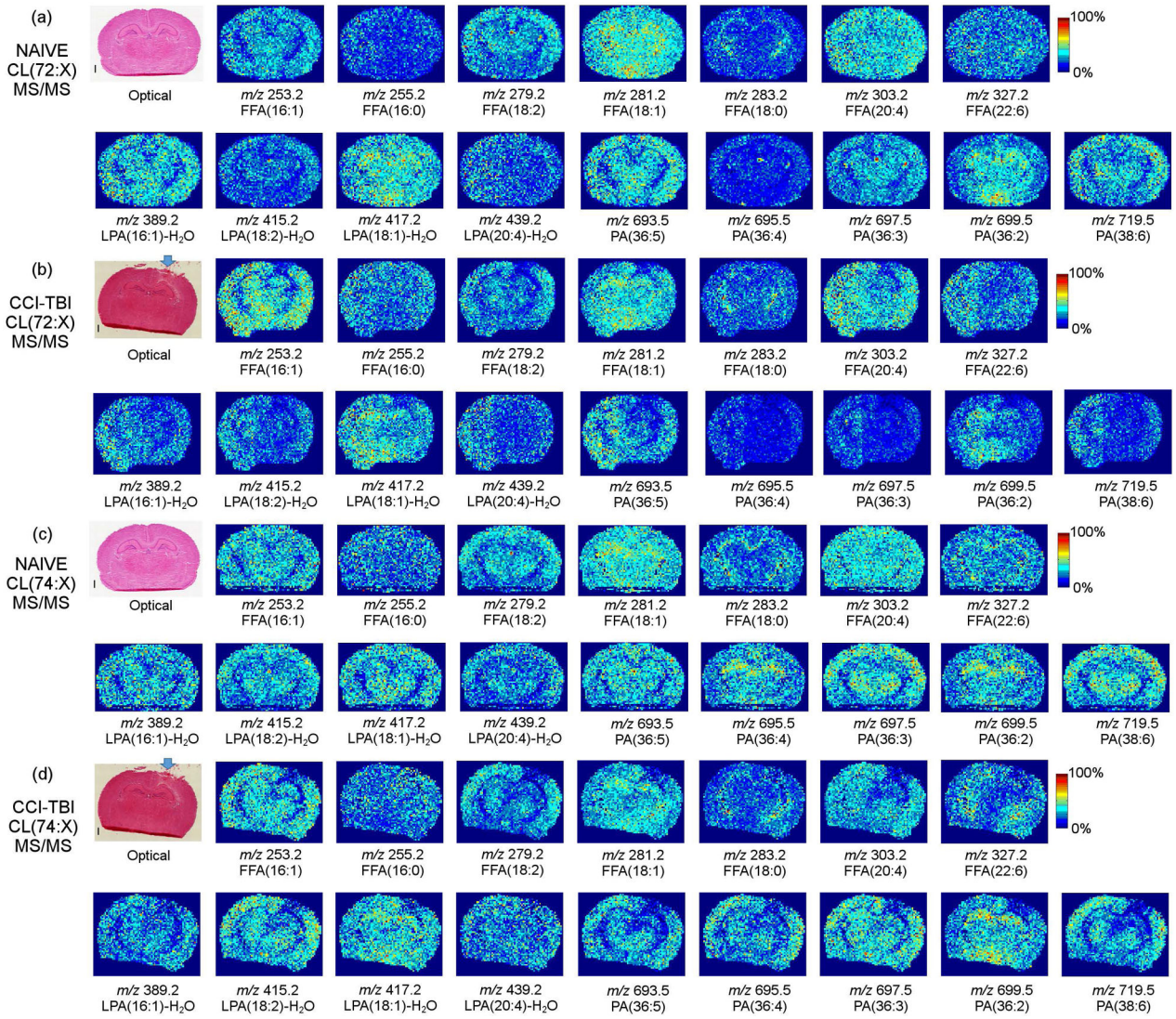

Fig. 5. MALDI-MSMS images of the CL (72:X) and (74:X) clusters in naive and CCI-TBI rat brain tissue

MS/MS analysis was performed on the CL cluster (72:X) centered around *m/z* 1448 for entire naive **(a)** and CCI-TBI **(b)** rat brain tissue coronal sections (representative images from 2 animals each, CCI and naive). A corresponding H&E optical image (scale bar = 1 mm) is shown for naive and CCI-TBI tissue. Heat maps for $[M-H]^-$ product ions of *m/z* 253.2, 255.2, 279.2, 281.2, 283.2, 303.2, 327.2, 415.2, 417.2, 693.5, 695.5, 697.5. 699.5 and 719.5 are shown which correspond to fatty acyl fragments 16:1, 16:0, 18:2, 18:1, 18:0, 20:4, 22:6, LPA (18:2)-H_2O, LPA (18:1)-H_2O, PA (36:5), PA (36:4), PA (36:3), PA (36:2) and PA (38:6), respectively. Spatial resolution = 200 microns. Arrow indicates the point of impact for the CCI tissue section. MALDI-MS images are displayed as relative intensities. MS/MS analysis was performed on the CL cluster (74:X) centered around *m/z* 1476 for entire naive **(c)** and CCI-TBI **(d)** rat brain tissue coronal sections. A corresponding H&E optical image (scale bar = 1 mm) is shown for naive and CCI-TBI tissue. Heat maps for fragments are the

same as indicated above. Spatial resolution = 200 microns. Arrow indicates the point of impact for the CCI tissue section. MALDI-MS images are displayed as relative intensities.

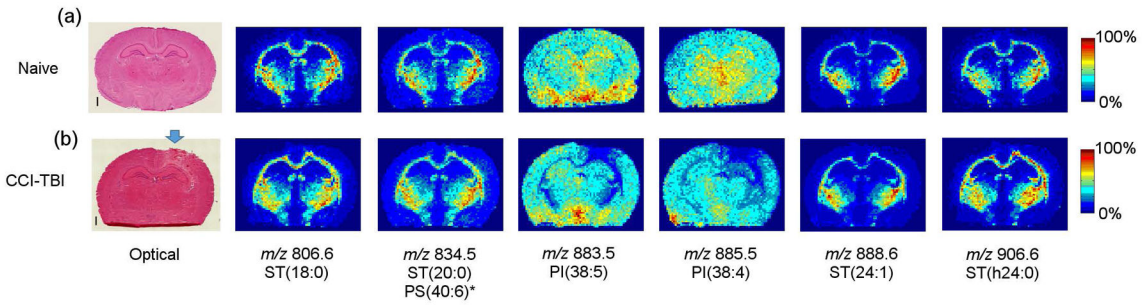

Fig. 6. MALDI-MS images of the major PI and sulfatide species from rat brain tissue

IMS negative ion mode heat maps of the major PI and sulfatide species in naive and CCI-TBI rat brain tissue sections treated with EDC-PLC (representative from 3 animals each, CCI and naive). A corresponding H&E optical image (scale bar = 1 mm) is shown for both naive and CCI-TBI tissue. Anionic lipid $[M-H]^-$ species include sulfatide (ST) 18:0, *m/z* 806.6; ST (20:0), *m/z* 834.5; ST (24:1), *m/z* 888.6; ST (h24:0), *m/z* 906.6; phosphatidylinositol (PI) 38:5, *m/z* 883.5 and PI (38:4), *m/z* 885.5. Arrow indicates the point of impact on the CCI tissue. ***** Indicates *m/z* 834.5 is isobaric with a PS (40:6) species. Spatial resolution = 200 microns. MALDI-MS images are displayed as relative intensities.